Chapter 13

Synthesis and Characterization of Advanced Carbon-Based Nanowires – Study of Composites Actuation Capabilities Containing These Nanowires as Fillers

V. Salles, L. Seveyrat, T. Fiorido, L. Hu, J. Galineau,
C. Eid, B. Guiffard, A. Brioude and D. Guyomar

Additional information is available at the end of the chapter

http://dx.doi.org/10.5772/54384

1. Introduction

Electromechanical properties in polymers can be employed to create a large number of sensors and actuators [1-2]. For example they could replace the piezoelectric materials commonly used in Micro Electromechanical Systems (MEMS). Even if the electromechanical coupling is relatively weak for polymers, they can generate high strains due to electrostrictive and Maxwell effects which are a quadratic function of the applied electric field as opposed to a linear function for piezoelectric materials. Other advantages of the polymers are their ease of processability, flexibility and cheapness.

Actuation capabilities of polymers depend on their intrinsic electrical, dielectric and mechanical properties. In order to optimize these properties, one way consists on the incorporation of nano-objects in the polymer matrix. Due to the nanometer-scale of the fillers dimensions, an important change of the properties can be obtained with relatively low ratios. In addition, the effect is more pronounced for conductive nano-objets since higher permittivities are expected to be obtained with a reduced amount of fillers [3]. Carbon-based nanocomposites are good candidates for electroactive nanocomposites: some studies were performed particularly on carbon black, carbon nanotubes, graphite or graphene fillers [4-9]. This part of the chapter is devoted to the influence of carbon-based nanowires (SiC@C, SiC@SiO_2, Fe_3C@C) as fillers on polyurethanes. The microstructural, dielectric, mechanical, electromechanical and electromagnetic properties are presented and discussed in the following sections.

Among the available electroactive polymers, polyurethanes are of great interest for a wide range of actuator applications due to their significant electric field-induced strains [10-11].

The total electrical field induced strain S can be expressed from electrostricition and Maxwell stress [12-13].

$$S = S_{electrostriction} + S_{Maxwell} = M^*_{33} E^2 \tag{1}$$

With M^*_{33} is the apparent electromechanical coefficient and E the applied electrical field.

The Mawwell stress effect comes from the interaction force between the positive and negative charges present on the electrodes

$$S_{Maxwell} = -\frac{\varepsilon_r^{'} \varepsilon_0}{Y} E^2 \tag{2}$$

With ε'_r the real part of the polymer relative permittivity, ε_0 the vacuum permittivity, and Y the Young's modulus.

The electrostriction represents the coupling between the electrical polarization and mechanical response in the material and is related to the electrostrictive coefficient Q and the relative permittiy ε'_r.

$$S_{electrostriction} = Q \varepsilon_0^2 (\varepsilon_r^{'} - 1)^2 E^2 \tag{3}$$

It was shown in previous studies [4, 8, 14] that in such polymers as PU, the Maxwell stress can be neglected.

Based on experimental studies [12, 14-15], the Q coefficient is found to be inversely proportional to the product of the Young's Modulus and permittivity according to:

$$Q \propto \frac{1}{\varepsilon_0 \varepsilon^{'}_r Y} \tag{4}$$

As a consequence, an empirical proportionality relationship is also obtained for the M coefficient :

$$M \propto \frac{\varepsilon_0 (\varepsilon^{'}_r - 1)^2}{\varepsilon^{'}_r Y} \tag{5}$$

http://dx.doi.org/10.5772/54384

This chapter is divided into two main parts. The fabrication procedures and the characterization of the as-prepared nanowires are detailed in the first part whereas the second part is dedicated to show how these nanomaterials can act on the electromechanical properties of EAPs when they are introduced as fillers, demonstrating their high potentiality to fabricate innovative actuators.

2. Fabrication and characterization of carbon-based nanowires

Among the different fabrication processes able to lead to one-dimensional nanostructures, one can distinguish two main approaches: one based on vapour deposition and one other based on polymer pyrolysis, corresponding to two well-known methods presented in this paper: Chemical Vapor Deposition (CVD) and electrospinning (ES) respectively. The interest in studying such two processes lies on fabrication of nanofibers which tend to be mono-crystalline in the first case and more polycrystalline in the second one, with nano-sized crystals.

2.1. Elaboration and characterization of silicon carbide nanowires by CVD

We report here a simple process to fabricate SiC-based nanowires coated with either silica, SiC@SiO_2, or carbon, SiC@C. In both cases, SiC nanocables (NC) were prepared from solid precursors of Si and C, *i.e.* SiO(s) and polypropylene (PP) respectively [16]. These reactants are much cheaper compared to high-purity gaseous reactants used in conventional CVD syntheses. In a typical experiment, the experiments were carried out in a furnace equipped with an alumina tube. PP was placed in an alumina boat, followed by a second alumina boat containing an equimolar mixture of Si(s) and SiO_2(s) or simply a SiO(s) powder, which was partially covered by a graphite condensation plate (Figure 1). All of the experiments were conducted under argon at a very low flow rate (10 mL.min^{-1}), at 1400 °C during 10 h.

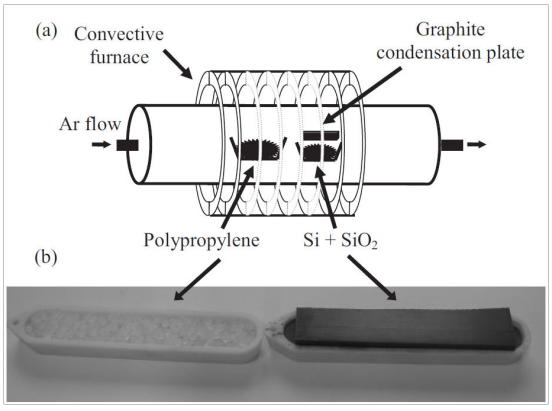

Figure 1. a) Experimental setup for the growth of SiC-based nanowires; b) Picture of the two alumina boats containing the reagents and the graphite condensation plate [16]

At high temperature, a reaction between Si and SiO_2 involves the formation of gaseous SiO which is able to react with carbonated species to initiate the nanowires growth. While using a PP/SiO weight ratio of 1 (maximum), SiC@SiO_2 NCs are formed whereas a ratio of 2 leads to the growth of SiC@C NWs (Figures 2 and 3). It is thus possible to control the silica thickness from 2 to 10 nm by adjusting the PP/SiO weight ratio from 1 to 0.25 for instance.

The as-obtained NWs have a diameter ranging from 20 to 40 nm. The NWs core consists of 3C-SiC, the cubic polytype of SiC, and the shell is either composed of amorphous silica (Figure 2) or turbostratic carbon (Figure 3). The high-purity of such structures was confirmed by EELS analyses and Raman investigations allowed to determine the P-type doping of the SiC-based NWs.

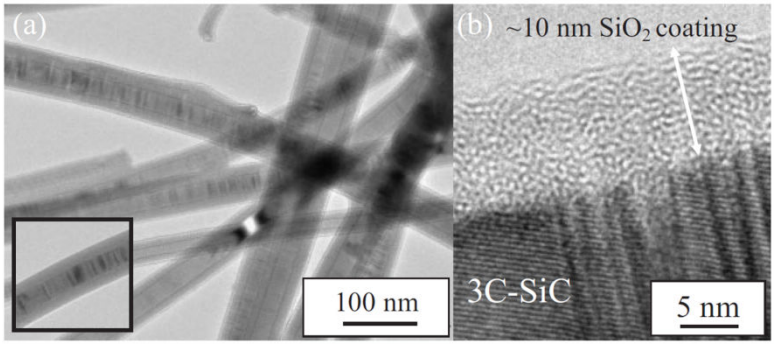

Figure 2. SiC@SiO2 NCs prepared from 1 g PP and 4 g SiO(s). a) Slightly out-of-focus TEM image of the crude product, where the amorphous silica layer can be easily distinguished from the SiC core (the corresponding well-focused image is included as an insert); b) HRTEM image showing a 10 nm silica layer around the SiC core [16]

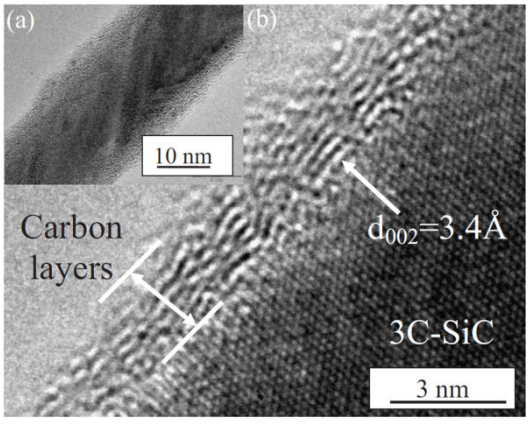

Figure 3. a,b) HRTEM images of a 30 nm SiC@C NC prepared by increasing the amount of PP to 8 g for every 4 g SiO(s) [16]

http://dx.doi.org/10.5772/54384

2.2. Elaboration and characterization of iron carbide nanowires by electrospinning

Electrospinning is a process which has been mainly studied and used during the last decade to prepare nanowires/nanofibers. We also have noticed an increasing interest of the scientific community during this period (Figure 4).

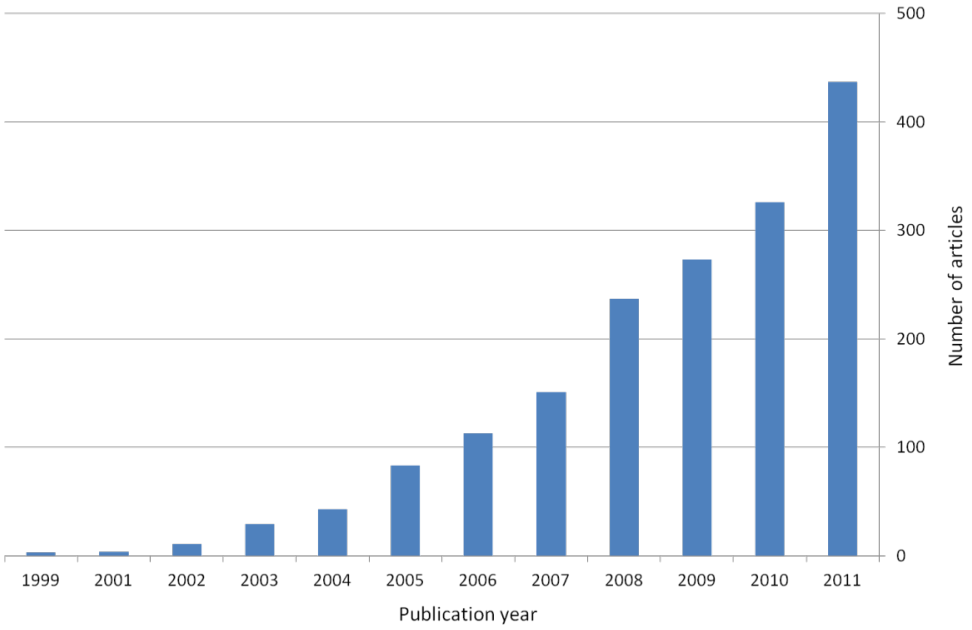

Figure 4. Histogram representing the number of scientific articles published per year during the last decade (Research performed on 4th June 2012 with "Web of Science", with "electrospinning" AND "nanofiber")

A lot of effort has been focused on the electrospinning process due to its versatility, which permits the formation of polymeric fibers as well as, after treatment, oxide and non-oxide inorganic fibers at submicro- and nanoscales [17-18]. This process is easy to scale-up to large amounts and has been recently employed to develop non-oxide ceramic nanowires. In this field, the synthesis of SiC [19-20], B_4C [21], B_4C/SiC [22], GaN [23] and BN [24] fibers has been reported for diameters smaller than 1µm. This production technique allows to precisely control the chemical composition of sub-microscale and nanoscale fibers which are serious candidate for applications ranging from smart textile to biomedical, including automotive and environmental areas.

Electrospinning consists in electrostatic stretching of a molten polymer or a solution containing a polymer solubilized in a solvent (the most common procedure). A high-voltage (HV) is applied between a spinneret (needle) and a metallic target (Figure 5).

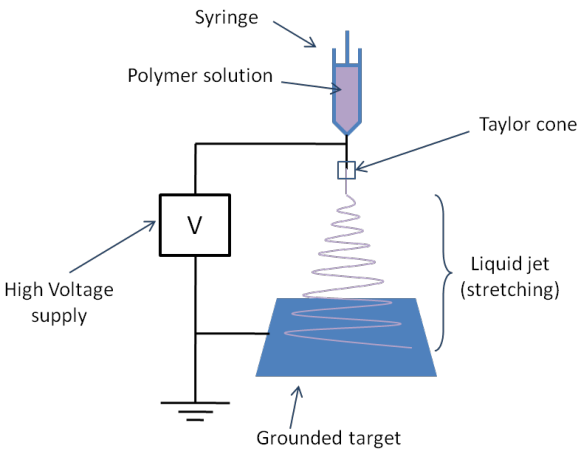

Figure 5. Schema of a typical electrospinning setup

With a low and continuous flow rate of solution through the needle, the solution drops without application of voltage but when the electric field is high enough to overcome the surface tension, a Taylor cone is formed at the needle tip and the solution is then accelerated toward the target in the form of a polymer jet. With stable working conditions, a continuous filament can be produced and collected as a solid 1D-material since the main part of the solvent evolves during the jet acceleration, in case of wet spinning. solvent evolves during the jet acceleration. Its final diameter, conventionally in the submicrometer scale, is about 1000 times lower than the inner spinneret diameter. Numerous parameters directly influence the morphology of the as-spun fibers/filaments. It is possible to fabricate dense, porous, beaded, flattened or perfectly cylindrical fibers simply by adjusting the solution properties :

- surface tension,
- electrical conductivity,
- viscoelastcity,
- polymer concentration,
- solvent(s) volatility,

and/or the spinning conditions :

- high-voltage,
- working distance,
- polymer/solution flow rate,
- inner needle diameter,
- type of target,

http://dx.doi.org/10.5772/54384

• moisture degree.

In case of fabrication of inorganic fibers by electrospinning, a specific precursor is employed [17-24]. Iron-based materials (iron oxide and iron carbide) can be fabricated from a mixture of polyvinyl pyrrolidone (PVP), bringing the spinnability property, and iron (II) acetate ($FeAc_2$) in acetic acid and ethanol (Figure 6) [25].

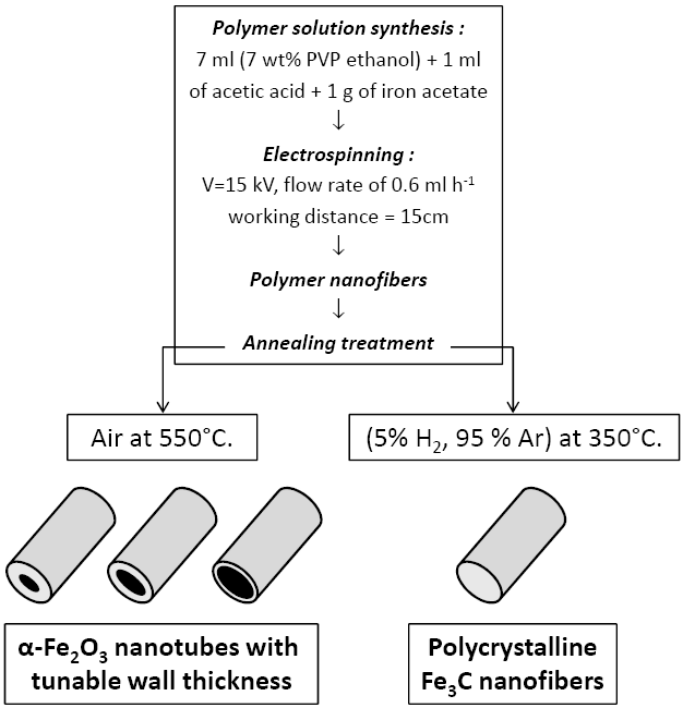

Figure 6. Experimental process with the different nanostructures obtained [25]

After stirring, to obtain a homogeneous and brown colored solution, the polymer solution is loaded into a syringe (5 mL) before being spun on a metallic target. After optimization of all spinning parameters, homogeneous filaments characterized by a smooth surface and an average diameter ranging from 200 to 500 nm can be obtained according to the precursor content (*i.e.* $FeAc_2$/PVP ratio) in the initial solution (Figure 7). An average value was calculated on 100 fibers of each sample giving a linear evolution of the fiber diameter versus the $FeAc_2$/PVP ratio: 440 nm, 395 nm, 260 nm and 220 nm for ratios of 2.63, 1.75, 0.87 and 0.43 repectively. This phenomenon is mainly attributed to a decrease of solid content when the ratio is decreased since the PVP content is the same in all the solutions (corresponding to 7 wt%). We can notice that iron acetate is stored and sampled under argon in order to prevent it from degradation over time.

A pyrolysis step was then carried out under argon and hydrogen (95% Ar and 5% H_2) with a heating rate of 3°C/min and an holding time of 4h at 450°C before cooling down. This thermal treatment allowed the organic part decomposition as well as the precursor conversion into an inorganic material. The thermal behaviour of the filaments during the pyrolysis step is still under investigation but we know that the last weight loss is due to PVP gaseous evolution up to 400-450 °C. Above this temperature, there is no more weight variation of the filaments. Temperatures above 800 °C were not studied.

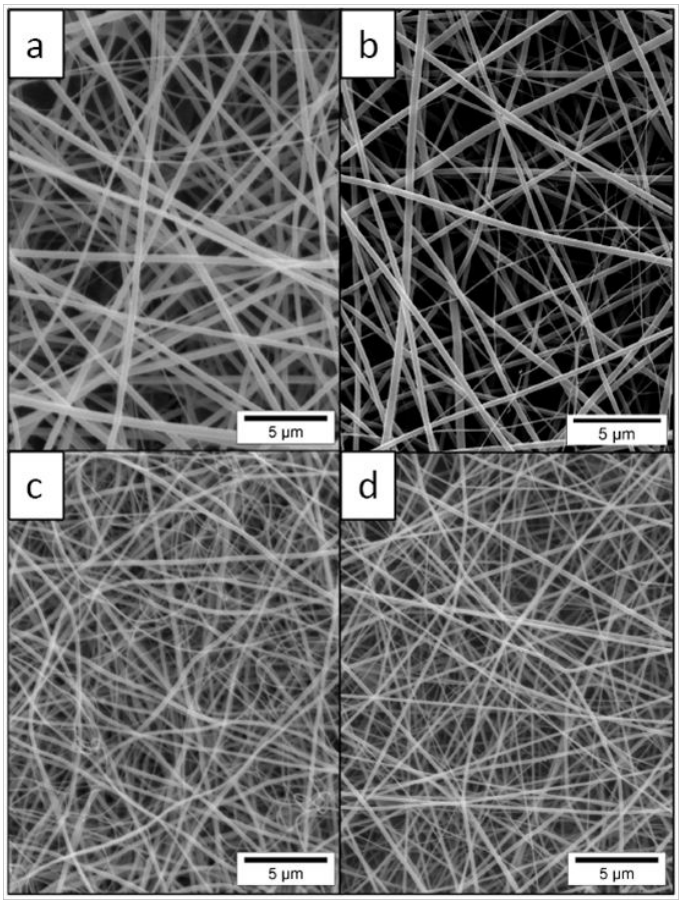

Figure 7. SEM images of the various PVP/$FeAc_2$ nanofibers with different wt ratios (FeAc2/PVP). (a) ratio = 2.63; (b) ratio = 1.75; (c) ratio = 0.87; (d) ratio = 0.43 [25]

http://dx.doi.org/10.5772/54384

The weight loss occuring during treatment is logically accompanied by a shrinkage in the macroscopic sample dimensions (already high-lighted and described in a previous work [24]), as well as in the filament diameter (Figure 8).

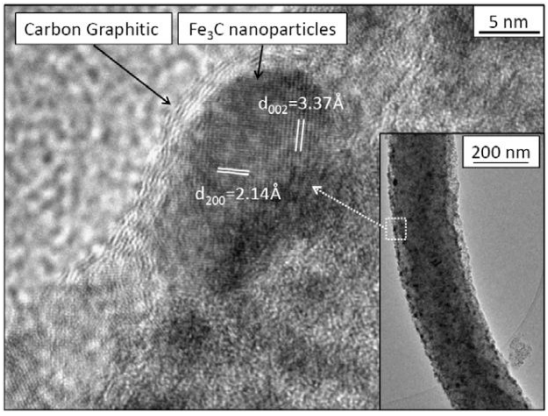

Figure 8. HRTEM of Fe_3C nanoparticles surrounded with graphitic planes. Inset: TEM images of Fe_3C nanofibers prepared with $FeAc_2$/PVP = 0.87 [25]

As XRD analysis was inadequate (no signal) to characterize the type of material composing constituting the inorganic filaments, transmission electronic microscopy (TEM) was performed on several filaments (Figure 8). The first main information is that the filaments are made of nanoparticles homogeneously dispersed in a matrix made of a different material. High-resolution TEM (HR-TEM) was then used to observe that the small nanoparticles have a spherical shape, and interplanar distances of 3.37 and 2.14 Å both measured on the same nanoparticle indicating the presence of pure iron carbide, corresponding to crystalline planes (002) and (200), repectively, of the Fe_3C orthorhombic phase. Moreover, these cementite domains are surrounded by well-known concentric graphitic planes forming a coating layer of 2-3 nm on the particle surface. The reduction in a hydrogen atmosphere of the as-electrospun PVP/$FeAc_2$ fibers is responsible for the formation of polycrystalline Fe_3C nanofibers embedded in carbon graphitic planes, ensuring stability and cohesion of the Fe_3C nanoparticles. The presence of graphiic carbon was confirmed by Raman spectroscopy with D and G bands at 1360 and 1594 cm^{-1} respectively [25].

The functionalization of organic matrices for electroactuation application has been studied and is presented below, using either SiC-based or Fe_3C-based nanowires as inorganic fillers. Carbon-based fibers, SiC@C and Fe_3C, were expected to be interesting because of their carbon coating which should enhance the surface electrical conductivity of the fillers, thus promoting the charge displacement at a nano- or a submicro-scale inside the polymer matrix. This should have a positive effect on the electrical polarization of the polymer host, directly linked to its ability to be deformed when it is subjected to an electric field.

3. Integration of the nanowires into polymer and study of composites actuation capabilities

3.1. Elaboration of nanocomposites

The two polymers were polyether-based aromatic thermoplastic polyurethane (PU), purchased from Lubrizol Corporation: Estane 58888 NAT 0.21 (PU88) and Estane X-4977 NAT039 (PU75). They differ by the ratio of hard to soft segments. Hard segments (HS) comprise the 4.4′ methylene bis(phenyl isocyanate) (MDI) and 1,4-butanediol (BDO) and soft segments are poly(tetramethlene oxide) (PTMO). The PU88 has a density of 1.13 g/cm^3, a hardness of 88 shore A and the HS content is about 46%; the PU75 has a density of 1.07 g/cm^3, a hardness of 75 shore A and the HS content is less, near 26% [26]. HS amount is an important factor because the physical properties depend directly on the degree of phase separation between the hard and the soft phases.

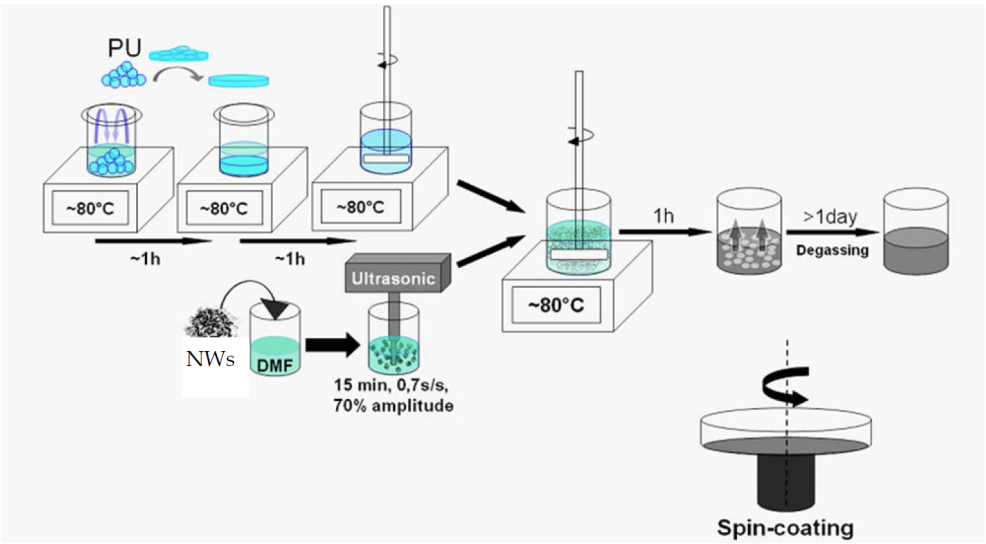

Figure 9. Elaboration of the PU88-SiC nanocomposite solution by solution casting method and spin coating [26]

PU88-SiC@C and PU88-SiC@SiO_2 nano-composite films were prepared following a solution casting method (Figure 9). Before use, the PU granules were heated at 80°C for 3 h to remove any traces of water. They were then put in N,N-dimethylformamide (DMF, Sigma-Aldrich D158550, 99%). The solution was maintained at 80°C for 2 h. The SiC nanowires were dispersed into DMF using an ultrasonic processor (Hielsher UP400S, 400 W, 24 kHz, 7 mm diameter sonotrode) under the following experimental conditions depending on the type of the nanowire: 10 to 20 min duration, 80% amplitude, 80% pulse. This solution was added to that of the polymer and the resultant mixture was heated at 80 °C for 1 h under mechanical stirring, until a homogeneous and viscous solution was obtained. This solution was de-

http://dx.doi.org/10.5772/54384

gassed for 24 hours at room temperature before spin coating on glass plates using a Laurell WS400 BX spin coater. This was a two steps process of 10 and 15 seconds with different rotational speed depending on the desired thickness: 200/300 rpm for 80 μm and 500/800 rpm for 35 μm. The films were then placed in an oven at 60°C for 24 hours and then removed from the glass substrate. A second heating treatment at 125°C (below the melting temperature) for 3 hours was performed in order to eliminate any residual traces of solvent.

The elaboration method was improved for the PU75-Fe_3C@C nanocomposites by using closed recipients during the dissolution and mixing steps so that the evaporation of the DMF solvent was avoided. In addition, the solution was applied on glass plates with an Elcometer 3700 doctor blade film applicator (Figure 10). This technique produced large surface films with homogeneous thickness. The following thermal treatments were the same as described above.

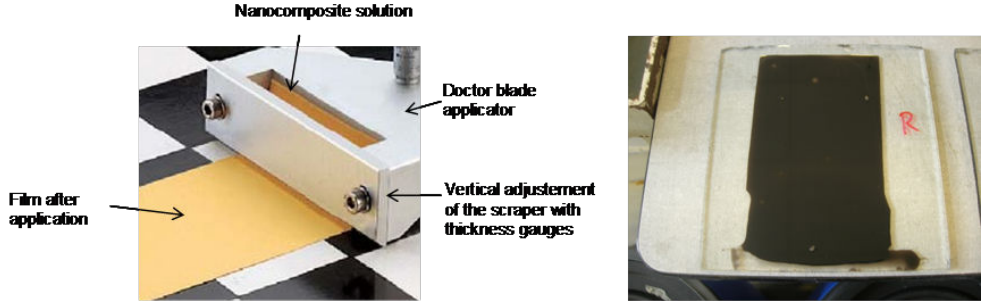

Figure 10. Deposition of the PU75-Fe_3C nanocomposite solution with Elcometer 3700 doctor blade applicator

For both methods (Figures 9 and 10), the weight fractions of fillers varied between 0 and 4 %.

It is important to note that spin coating is widely used as a shaping method for EAPs that are introduced inside actuators devices, however, the method so-called "Doctor Blade" allows to prepare polymer or composite films with larger dimensions which is interesting for studies necessitating numerous samples for analyses (electrostriction, mechanical test, DSC, SEM,...), with verification of reproducible results as well.

3.2. Characterization of the nanocomposites

3.2.1. Structural characterization of the nanocomposites

Microstructural observations (Figure 11), carried out by SEM using a cryo-fracture preparation, showed that the nanowires seem to be aligned preferentially in planes parallel to the surface of the film. Whatever the shaping method used, taking into account the external forces applied on the long chains of PU, it is assumed that there is no difference of the nanowires organization in the polymer host. The homogeneity of this distribution was checked over the entire width, and from the bottom to the top surface.

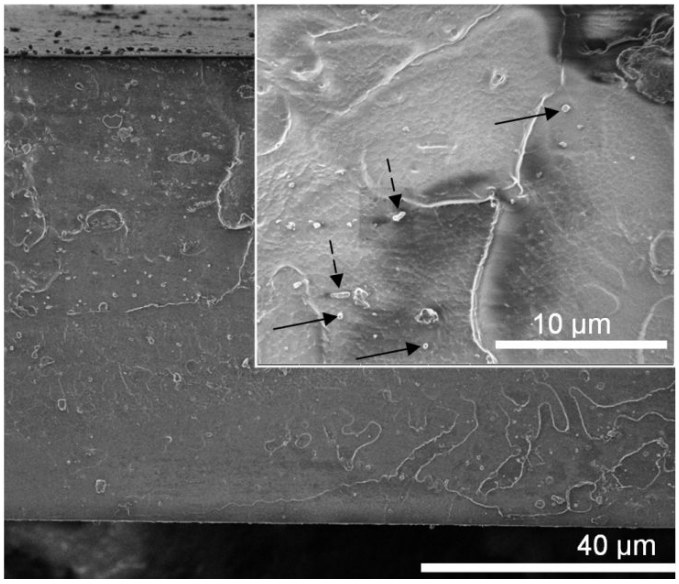

Figure 11. SEM observations performed on samples PU75-Fe_3C (2.5 wt% of Fe_3C); Arrows indicate the presence nano-fillers with perpendicular (solid arrows) and non perpendicular (dashed arrows) orientations compared to the fracture plane

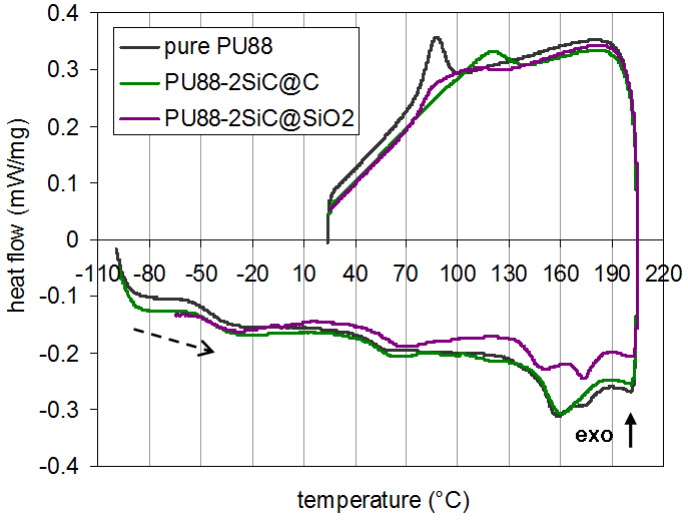

Figure 12. DSC thermograms on heating and cooling of pure PU88, PU88-2SiC@C and PU88-2SiC@SiO_2 nanocomposites films

http://dx.doi.org/10.5772/54384

The Differential Scanning Calorimetry (DSC) technique was used to study the effect of the nanowires on the structure of the host polymer. The thermal analysis was performed with DSC 131 evo from Setaram, under nitrogen atmosphere. The samples (about 20 mg) were placed in closed 100-µl aluminum crucibles and cooled from ambient temperature down to -100°C, then heated to 210°C and finally cooled to RT. The heating and cooling ramps were performed at 10°C.min^{-1}.

The thermograms for the pure PU88, and the PU88-2SiC@C and PU88-2SiC@SiO_2 compositions are presented below (Figure 12).

The glass transition temperature for the soft segments (Tg), melting temperatures (T_{II} and T_{III}), heat of fusion (ΔHm), crystallization temperature (T_c) and heat of crystallization (ΔHc) are summarized in Table 1.

	Tg (°C)	T_{II} (°C)	T_{III} (°C)	ΔHm (J/g)	T_C (°C)	ΔHc (J/g)
Pure PU88	-42.5	157	173	9.6	88	-8.6
PU-0.5SiC@C	-40.8	159	173	8.9	111	-9.9
PU-1SiC@C	-40.0	157	174	10.1	115	-8.8
PU-2SiC@C	-42.0	160	172	8.3	118	-8.4
PU-3SiC@C	-43.1	160	174	8.8	119	-7.0
PU-1SiC@SiO_2	-40.9	150	173	8.9	88-110	-10.7
PU-2SiC@SiO_2	-47.6	158	173	10.0	88	-10.4
PU-3SiC@SiO_2	-48.3	153	171	10.4	88-110	-11.5
PU-4SiC@SiO_2	-39.6	150	171	10.3	110	-11.8

Table 1. DSC results obtained for the PU88-SiC nanocomposite films

The first thermal phenomenon near -45°C was related to the glass transition (Tg_{SS}) of the soft segments (SS). This value can give an estimation of the amount of hard segments (HS) dissolved in the soft domains and as a consequence an indication of the purity of the soft phase [27-28]. When the fraction of nanowires was increased, no significant change of Tg was observed. It was thus concluded that the degree of HS-SS mixing was not modified by the incorporation of nanowires.

Some effects of relaxation of the polymer chain, a modification at the SS/HS interface or thermal endotherm seemed to explain the behavior of heat flow near 60°C. At temperatures in the range 150-170°C, it was observed a bimodal endotherm that can be related to the micromixing of non-crysytalline or semi-crystalline hard and soft phases followed by the melting of crystalline HS [29]. Another interpretation of the bimodal peak could be the melting of crystalline hard segments: the two peaks represent the two characteristic lengths of HS [27]. In both cases, the increase of the samples' crystallinity would be accompanied by an increase of these temperatures and/or an increase of the total enthalpy of the 2 phenomena.

With the incorporation of SiC@C nanowires, the endothermal peaks remained unmodified, temperature and corresponding enthalpy did not change. With SiC@SiO_2, one can observe only a slight decrease of the temperature of the first endotherm related to the micromixing of hard and soft phases.

During the cooling experiments, a more important influence of the nanowires on the crystallization behavior was observed. When the amount of nanowires was increased, the crystallization temperature was raised but without a significant change in enthalpy. The nanowires seemed to act as nucleating agents improving the crystallization. There is a more important effect on the crystallization of the polyurethane with the incorporation of SiC@C compared to SiC@SiO_2 (Figure 12).

The same study has been performed on nanocomposite films based on PU75 and Fe_3C@C nanowires and the values of Tg and melting temperatures and heat of fusion are summarized in Table 2. The PU75 is less rigid than the PU88, as indicated by the value of the glass transition temperature which is 25°C under the PU88 one. With the incorporation of Fe_3C@C, there is no modification of the thermal properties during heating and cooling, and so no morphological change of the PU75 polymer host.

	Tg (°C)	T_{II} (°C)	T_{III} (°C)	ΔHm (J/g)
Pure PU75	-68.6	153	174	2.3
PU75-2.5Fe_3C@C	-69.0	152	175	3.0
PU75-5Fe_3C@C	-71.7	152	174	2.4

Table 2. DSC results obtained for the PU75-Fe_3C@C nanocomposite films

It can be concluded from these DSC results that, whatever the PU, no major microstructural modification of the matrix was observed with the incorporation of nanowires.

3.2.2. Dielectric properties of the nanocomposites

Prior to the electrical measurements, the samples were coated with 20 nm thick gold by sputtering. The relative permittivity ε', the dielectric loss factor tan δ and the real part of the electrical conductivity σ' were obtained with a Solartron 1255 impedance / gain-phase analyzer and a 1296 dielectric interface. The voltage was set at 1 V_{RMS} and a frequency range was performed in the range 0.1-10^5 Hz.

Figure 13 presents the electrical conductivity versus frequency of some PU88/SiC nanowires composites. In all samples, two frequency regions can be observed: one for which the conductivity was almost constant (low frequencies < 10Hz) and which is attributed to charge displacements and another one (high frequencies > 10Hz) where the conductivity increased with the frequency and corresponds to the dielectric losses [30].

Compared to the SiC@SiO_2, the SiC@C nanowires lead to a slightly more important increase of the polyurethane conductivity. This is in goog agreement with the conductive carbon layer which covers the SiC wires, instead of the SiO_2 one.

http://dx.doi.org/10.5772/54384

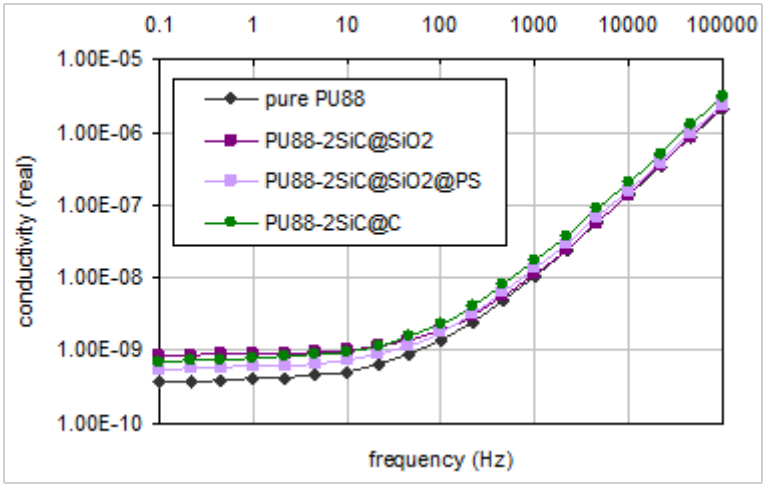

Figure 13. The electrical conductivity versus frequency for pure PU and PU88-2SiC composites

The frequency/conductivity curves show that even if the conductivity is slightly enhanced with the incorporation of nanowires, the percolation threshold is not reached even with higher concentrations of SiC (3% tested) or SiO_2 (4% tested). This threshold could be estimated as the content located between that for which the conductivity still depended on the frequency and that for which it became completely independent of the frequency.

Figure 14 exhibits the permittivity versus frequency of some PU88/SiC nanowires composites

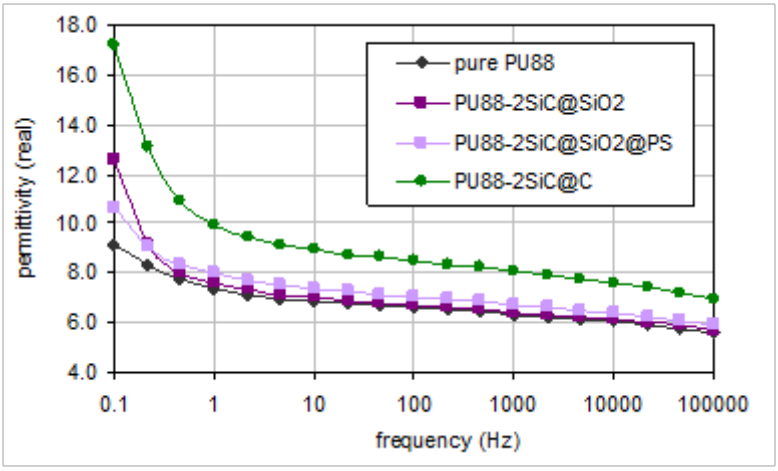

Figure 14. The relative permittivity versus frequency for pure PU and PU88-2SiC composites.

Whatever the sample, the permittivity increases as the frequency is lowered, which is in good agreement with Maxwell Wagner mechanism [31]. The composites present an higher permittivity than the pure polyurethane one: for example, at 0.1 Hz, it increases from 9 for pure PU to 12 for PU88-2SiC@SiO_2 and to 18 for PU88-2SiC@C.

The effect is more pronounced for the SiC@C compared to SiC@SiO_2 certainly because the first type of filler has a conductive carbon layer on the surface instead of the insulating SiO_2 layer.

For the PU75-Fe_3C system, the same dielectric characterization was made (Figure 15).

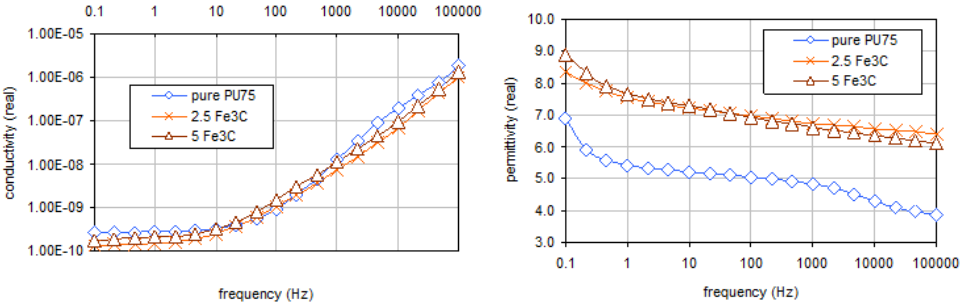

Figure 15. The conductivity (a) and relative permittivity (b) versus frequency for composites with varying SiC contents (a) PU88-SiC@C and (b) PU88-SiC@SiO_2

The conductivity curves for the PU75 system shows like for the PU88 two regions depending on the value of the frequency. Whatever the frequency, the conductivity is not really modified with or without Fe_3C.

Compared to the SiC@C filler, the Fe_3C@C has a very slight influence on the permittivity of the samples at low frequency. But at a frequency near 1 kHz, the gain was of the same order of magnitude for the two fillers i.e. 1.35 fold.

3.2.3. Mechanical properties of the nanocomposites

The mechanical behaviour of the composite films was evaluated on 25 x 10 mm^2 samples, using a house made tensile test (Figure 16). On one end, the sample was clamped onto a Newport platin and the other end onto a force sensor. The stage was moved using a function generator at a frequency of 50 Hz and the dynamic force was acquired on an oscilloscope. Measurements were performed over a deformation range from 0 to 100%. The Young's modulus was determined at the beginning of the curve strain / stress for elongations less than 4%.

Figure 17 exhibits the evolution of the Young's modulus of the nanocomposites films as a function of the content of nanowires.

http://dx.doi.org/10.5772/54384

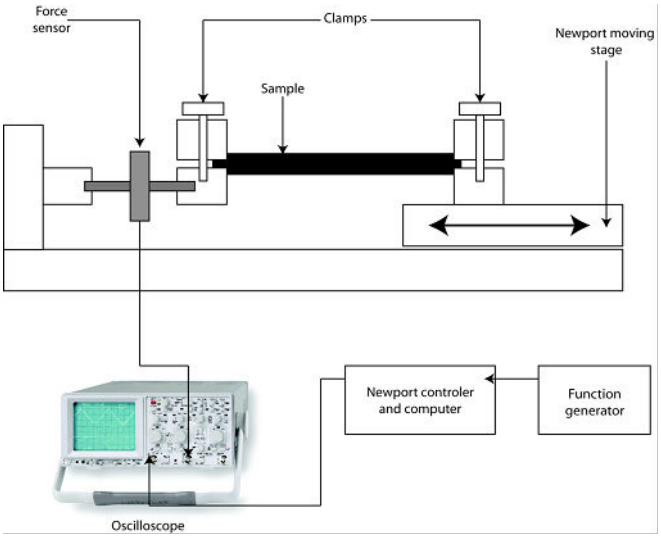

Figure 16. Experimental set-up for measuring the mechanical properties of the nanocomposite films

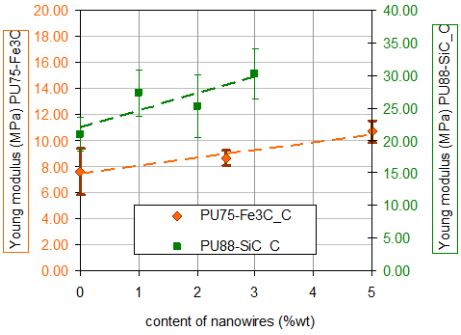

Figure 17. The Young's modulus versus the content of nanowires for PU88-Si@C and PU75-Fe_3C@C

For the two polyurethane systems, it is observed an expected little increase of the Young's modulus with the incorporation of nanowires. For the same content of nanowires, for example 2.5%, there is a 1.3 gain factor for PU88-SiC@C and 1.2 gain factor for PU75-Fe_3C@C.

3.2.4. Electromechanical capabilities

a. Electric field-induced thickness strain measured by a double-beam interferometer at low frequency (0.1Hz).

The electric field-induced thickness strain S was measured with a double-beam laser interferometer (Agilent 10889B), with a precision in the order of 10 nm. The film samples of 25 mm diameter were placed on a horizontal stainless steel disc (20 mm in diameter), and a second brass disc placed on the upper side of the film allowing the application of a bipolar electric field at 0.1 Hz. The voltage was supplied by a function generator (Agilent 33250A) amplified 1000-fold through a high-voltage lock-in amplifier (Trek 10/10B). A guard ring was added to the sample surface and grounded so as to eliminate any surface leakage currents. Figure 18 gives photographs of the experimental set-up for strain measurements.

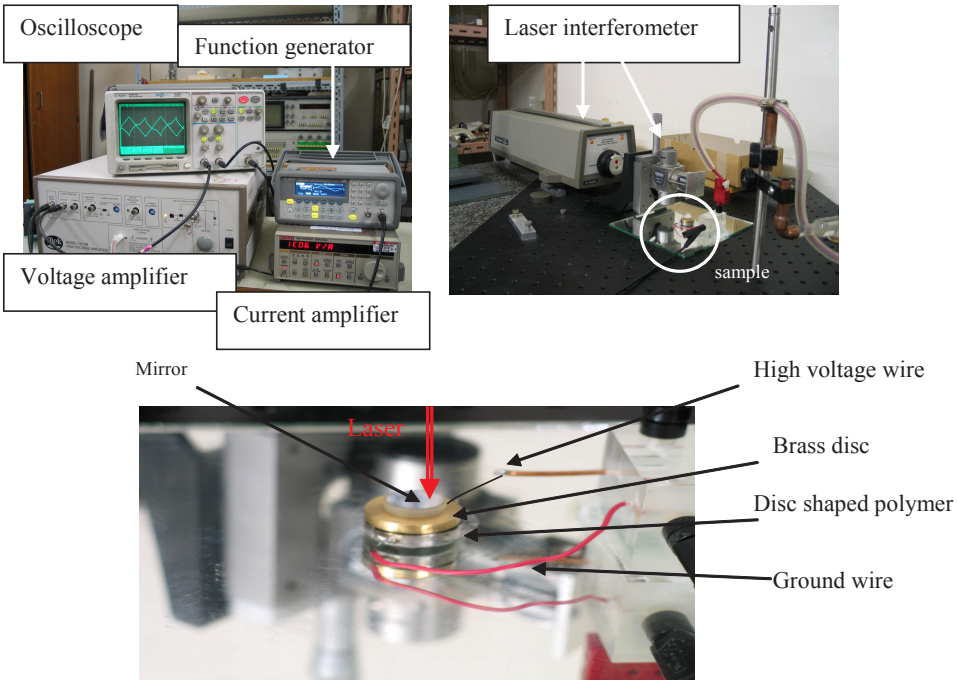

Figure 18. Experimental set-up for strain measurements with laser interferometer at 0.1 Hz.

Figure 19-a) presents the thickness strain amplitude – S_3 (S_3 is negative since the film is compressed) versus the electric field amplitude of pure and filled with 0.5% SiC@C PU88 films of different thicknesses.

All studied films exhibited the same type of strain variations (except the 20 μm – thick nanocomposite because electric breakdown occurred above 18V/μm): a first region where the strain increases regularly with the electric field amplitude indeed and a second region at higher fields where an asymptotic value is reached. This is the result of the hyperelastic behaviour of such PU materials.

http://dx.doi.org/10.5772/54384

The deformation depends on the thickness of the film: lower electric fields were required to obtain a given strain level before saturation as the film's thickness increased. The 20µm-thick nanocomposite film presented the maximal thickness strain of about 18% at 18 V/µm. At moderate electric values, the greatest effect was observed for the 100 µm-thick PU-SiC@C film since the strain was equal to 10% at a field as low as 6 V/µm.

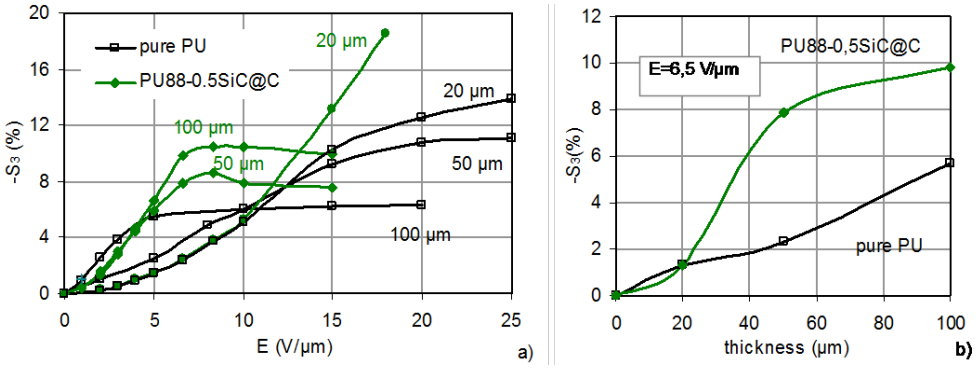

Figure 19. Evolution of the strain amplitude versus the electric field amplitude for various thicknesses of pure PU88 and PU88-0.5SiC@C films at 0.1 Hz. (b) The evolution of the strain amplitude versus the thickness of pure PU88 and PU88-0.5SiC@C films at E= 6.5 V/µm [11]

As the relative permittivity was found to be higher in the SiC@C composites, the results showed an increase of the interfacial polarization induced by a pronounced space charges effect. Space charges accumulate in PU and more effectively in PU-SiC@C composites and it was still evidenced by the large dependence of the strain on the film thickness, particularly for low and medium electric field values (E < 10 V/µm). These charges are generally electrons injected in the bulk from the electrodes and/or impurities (ions) in the sample which are trapped to the different structural interfaces of the material. The consequence of the presence of space charges is the appearance of high electric field local densities, located at the various trapping sites (defects, interfaces), thus yielding a non-uniform field distribution in the film thickness and consequently a high deformation [32].

However, the film must be thick enough to present such a strain improvement by space charges effect, as it is shown in Figure 19-b which gives the evolution of strain at 6.5 V/µm electric field versus thickness. If the film was too thin, the strain was not increased because the interfaces that were able to trap the space charges started to overlap and as a consequence charge homogenization occured [14, 33]. When the film thickness increased, the strain also increased, with a more pronounced effect for the nanocomposite. It should be emphasized that the polyurethane exhibited a considerable ability to collect space charges certainly due to the two-phase structure composed of hard and soft segments inducing many interfaces. The presence of space charges were experimentally evidenced by studying the steady-state current – electric field characteristic of the films [11].

DSC measurements presented in previous section were performed in order to determine whether the SiC@C nanowires themselves or polymer chains/nanowires' interfaces behaved as additionnal space charge traps and/or if they increased the level of phase mixing between soft and hard segments and consequently the structural interface density. The DSC results show that there is no modification of the phase mixing so it can be concluded that space charge effects in the composites were not enhanced by an increase of the structural interface density, but rather by the SiC@C nanowires themselves, acting as charge traps.

Another study was performed with SiC@SiO_2 nanowires as fillers with the laser interferometer method at low frequency [34]. The electric field induced thickness strain response has been investigated for the polystyrene-grafted silica coating of SiC NWs (PU88-2SiC@SiO_2@PS) nanocomposites and compared to the pure polyurethane film and the PU88-2SiC@SiO_2 nanocomposite without polystyrene grafting.

Polyurethane polymer filling with both types of nanowires leads to a higher electromechanical response than for the pure PU88 film. At a moderate electric field of 10 V/μm, 2SiC@SiO_2@PS loading increased the strain level of pure PU88 by a factor of 2.2. The improvement came partially from polystyrene grafting since the PU-2SiC@SiO_2 films showed only a 1.7 times increase. It was shown in the article that since a higher strain was observed for the PU88-2SiC@SiO_2@PS films, the polystyrene chains grafting seemed to act as a dispersing agent, thus yielding a homogeneous distribution of NWs in the composite.

b. Deflection strain under electric field of a diaphragm type dielectric actuator working at high frequency (near 1kHz).

Another way to investigate the electromechanical properties of polymer films is to measure the expension in the 31 direction (which is directly proportional to the 33 contraction). It was chosen to investigate it using a diaphragm, which is also a good candidates for integration of these polymer films into Microsystems [35].

The diaphragm device (Figure 20) comprised a sample holder and the electroded sample.

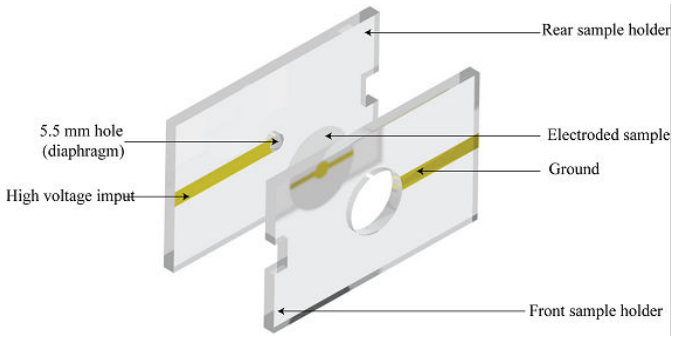

Figure 20. Diaphragm device used for the measurement of the deflection strain under electrical field at high frequency [35]

http://dx.doi.org/10.5772/54384

The sample holder was fabricated in thick PMMA sheets. Two diameter holes of 5.5 mm and 20 mm were drilled into the two parts of the device. The 5.5 mm hole constituted the diaphragm. Gold electrode was sputtered onto each part for electrical connections. Samples of 25 mm in diameter were electroded using gold sputtering as shown in the figure 19 and then aligned with the 5.5 mm hole and the electrode on the rear part of sample holder. The sample adhered onto the sample holder by electrostatic forces.

The polymer film was excited in a pseudo piezoelectric mode by applying a DC electrical field in addition to the AC excitation. The sinusoidal voltage was applied using a function generator (Agilent 33200A) and amplified by the Trek Model 10/10 high voltage power amplifier The DC component induces a constant polarization of the membrane, and thus, a piezoelectric behavior. In this study, all data were recorded in pseudo-piezoelectric mode and at the first resonant frequency. In addition, the DC bias voltage was chosen equal to the AC voltage magnitude. The membrane deformation was recorded using a Polytech OFV-5000 vibrometer equiped with a OFV-505 sensor head. The reflectivity of the gold electrode was used to monitor the deflection. The deflection strain is defined as S_d=S/d where d is the deflection and h the sample thickness. The deflection is caused by the compressive strain undergone by the film rigidily clamped at the edge.

The deflection strain magnitude for PU75 loaded with 0, 2.5 and 5wt% of Fe_3C@C has been studied as a function of the square applied electrical field magnitude [36]. The results are presented in figure 21.

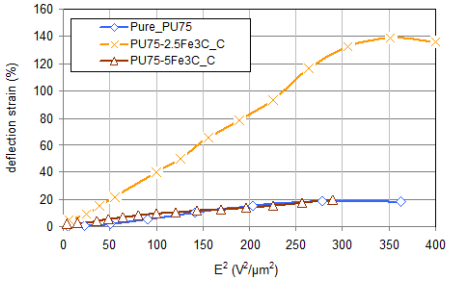

Figure 21. The deflection strain versus the square applied electrical field for PU75-Fe_3C@C nanocomposites films

At low and medium electric fields (E < 10 V/µm), the deflection strain increased quasi-linearly with E^2, thus confirming the electrostrictive nature of the electromechanical response. For higher electric field, a saturation effect corresponding to an asymptotic constant value of strain was observed and can be attributed to the saturation of the electrical polarization [37].

The deflection is increased by 2 to 7 fold from pure PU75 to 2.5% load PU depending on the electrical field magnitude, and is higher than that measured on the same PU filled with carbon black [35]. A considerable deflection strain of more than 130 % was found for the PU75-2.5Fe_3C@C nanocomposite for a 18 V/µm electrical field.

With higher amount of Fe_3C nanowires, the deflection decreases. This decrease could be related to an agglomeration of the nanowires. Some complementary structural charaterizations are under progress by SEM and Focused Ion Beam in order to fully understand this behavior. Even if the global permittivity and dielectric loss do not increase dramatically, it is possible that some agglomerates appear locally inside the film and contribute to decrease the interfacial polarization and consequently the density of trapped charges. This effect yields a decrease in the deflection strain amplitude.

By using the same method, measurements have been performed on different PU88-SiC@C nanocomposites. Figure 22 exhibits the strain deflection versus the square of the electric field. Even if the polyurethane host is not the same for the study, it is possible to compare the influence of the two types of nanowires, ie SiC@C and Fe_3C@C, on the actuation performances.

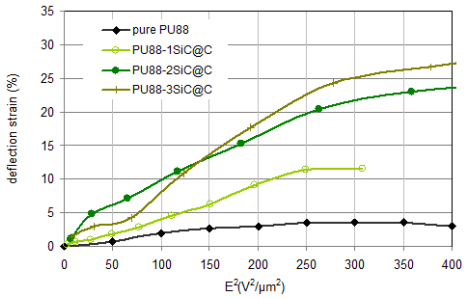

Figure 22. The deflection strain versus the square applied electrical field for PU88-SiC@C nanocomposites films

The electric field induced a deflection of PU88 films which was lower than that of the PU75 films; it is in agreement with a similar value of the relative permittivity in both cases and a lower value of Young's modulus of the PU75 films. Indeed the strain depends directly on the ratio of permittivity over Young's modulus as shown in the equation (5).

At high electrical fields, the PU88-3SiC@C shows a 25% deflection strain which is 6 times higher than for pure PU88. The gain in actuation is similar to that measured on PU75-2.5Fe3C@C. This is consistent with results presented in previous section: dielectric studies for both nanocomposites have shown an increase of the relative permittivity near 1 kHz with a gain of 1.35. Moreover, the mechanical reinforcement was also comparable for the 2 types of composite films.

4. Conclusions

Two different methods of synthesis were investigated and exploited to develop new carbon-based nanowires, SiC@SiO_2, SiC@C and Fe_3C, used as fillers in PU matrices to improve the deflection capabilities of these electroactive polymers.

http://dx.doi.org/10.5772/54384

Polyurethane composites filled with low amounts of SiC@C and Fe_3C@C nanowires (0 – 5 wt %) were prepared by two solvent methods and yielded to very large surface films in the range of 30-80 μm in thickness. It can be noted that the deposit way was different for the two systems: spin coating for PU88-SiC@C films and doctor blade application for PU75-Fe_3C@C, both methods being used for preparation of actuators made of polymers.

The dielectric properties were studied at different frequencies and showed an increasing of the relative permittivity of the composites with the amount of nanowires. Permittivity and conductivity results showed also that the percolation threshold was not reached whatever the studied system. The mechanical properties were performed by using a simple tensile test and it was shown that the increase in the Young's modulus induced by the nanowires was only moderate.

Based on DSC analysis, only a very slight modification of the polyurethane host was detected with the incorporation of the nanowires and no difference in the degree of hard segments/soft segments mixing was found.

The actuation capabilities were studied by measuring the strain under an applied electric field with two methods.

The first method consisted in the measure of the electric field-induced thickness strain S with a double-beam laser interferometer at low frequency (0.1 Hz). At a moderate electrical field (6V/μm), it was found a 3 fold increase of the electrostriction coefficient for only 0.5%wt of SiC@C into PU88 polymer. The polyurethane is a good candidate for electromechanical applications, it has a good ability to collect space charges due to its special structure consisting of a mixing of hard and soft segments. It was shown that the nanowires acted as charge traps and then enhanced the electrical field induced deformation.

The second method is to measure the deflection strain of a diaphragm type dielectric actuator working at high frequency (near 1kHz). The deflection strain was considerably enhanced with the incorporation of either Fe_3C@C and SiC@C nanowires into polyurethane films whatever the type of the polyurethane host. The maximum deflection strains measured at high electrical fields (18 V/μm) reached 130 % for the PU75-Fe3C@C nanocomposites and 25% for the PU88-3SiC@C. These values are considerable and at least 6 times higher than those obtained with corresponding pure polymer films.

Due to their evident large actuation capabilities, these new nanocomposites based on polyurethane and carbon-based nanowires are very promising materials for micro electromechanical systems.

Acknowledgments

Authors thank the Institut Carnot for its financial support and Veronique Perrin from LGEF (EA682 INSA Lyon) for mechanical tests and thickness strain measurements with laser interferometer. The authors also acknowledge the CTμ (Centre Technologique des Microstructures) of the Université Lyon 1 for access to the SEM.

Author details

V. Salles[1], L. Seveyrat[2*], T. Fiorido[1], L. Hu[1], J. Galineau[2], C. Eid[1], B. Guiffard[2], A. Brioude[1] and D. Guyomar[2]

*Address all correspondence to: laurence.seveyrat@insa-lyon.fr

1 Laboratoire des Multimatériaux et Interfaces, UMR 5615 CNRS, Université Lyon1, Université de Lyon, Bat. Berthollet, France

2 Laboratoire de Génie Electrique et Ferroélectricité, LGEF – INSA Lyon, France

References

[1] Bar-Cohen Y, Zhang Q. Electroactive Polymer Actuators and Sensors. MRS Bulletin 2008;33 173-181.

[2] Carpi F, Rossi D, Kornbluh R, Pelrine R, Sommer-Larsen P. Dielectric Elastomers as Electromechanical Transducers : Fundamentals, Materials, Devices, Models and Applications of an Emerging Electroactive Polymer Technology. Amsterdam: Elsevier Science; 2008.

[3] Nan CW, Shen Y, Ma J. Physical Properties of Composites Near Percolation. Annual Review of Materials Research 2010;40 131-151.

[4] Wongtimnoi K, Guiffard B, Bogner-Van de Moortèle A, Seveyrat L, Gauthier C, Cavaillé JY. Improvement of Electrostrictive Properties of a Polyether-based Polyurethane Elastomer Filled with Conductive Carbon Black. Composites Science and Technology 2011;71(6) 885-892.

[5] Park C, Kang JH, Harrison JS, Costen RC, Lowther SE. Actuating Single Wall Carbon Nanotube-Polymer Composites: Intrinsic Unimorphs. Advanced Materials 2008;20(11) 2074-2079.

[6] Zhang S, Zhang N, Huang C, Ren K, Zhang Q. Microstructure and Electromechanical Properties of Carbon Nanotubes/Poly(vinylidene fluoride-trifluoroethylene-chlorofluoroethylene) Composites. Advanced Materials 2005;17(15) 1897-1901.

[7] He F, Fan JT, Lau S. Thermal, Mechanical and Dielectric Properties of Graphite Reinforced Poly(vinylidene fluoride) Composite. Polymer Testing 2008;27(8) 964-970.

[8] Seveyrat L, Chalkha A, Guyomar D, Lebrun L. Preparation of Graphene Nanoflakes/Polymer Composites and Their Performances for Actuation and Energy Harvesting Applications. Journalf of Applied Physics 2012;111(10) 104904-104913.

http://dx.doi.org/10.5772/54384

[9] Guiffard B, Seveyrat L, Sebald G, Guyomar D. Enhanced Electric Field-Induced Strain in Non-percolative Carbon Nanopowder/Polyurethane Composites. Journal of Physics D: Applied Physics 2006;39(14) 3053-3057.

[10] Watanabe M, Hirai T, Suzuki M, Amaike Y. Electric Conduction in Bending Electrostriction of Polyurethanes. Applied Physics Letters 1999;74(18) 2717-2719.

[11] Guiffard B, Guyomar D, Seveyrat L, Chowanek, Bechelany, Cornu D, Miele P. Enhanced Electroactive Properties of Polyurethane Films Loaded with Carbon-coated SiC Nanowires. Journal of Physics D: Applied Physics 2009;42(5) 055503.

[12] Yimnirun R, Eury S, Sundar V, Moses PJ, Jang SJ, Newnham RE. Electrostriction Measurements on Low Permittivity Dielectric Materials. Journal of the European Ceramic Society 1999;19(6-7) 1269-1273.

[13] Pelrine R, Kornbluh R, Joseph J, Heydt R, Pei Q, Chiba S. High-field Deformation of Elastomeric Dielectrics for Actuators. Materials Science and Engineering 2000;11(2) 89-100.

[14] Guillot FM, Balizer E. Electrostrictive Effect in Polyurethanes. Journal of Applied Polymer Science 2003;89(2) 399-404.

[15] Diaconu I, David A, Dorohoi DO. An Experimental Investigation of Electroactive Polyurethane. Journal of Optoelectronics and Advanced Materials 2005;7(6) 2797-2801.

[16] Bechelany M, Brioude A, Stadelmann P, Ferro G, Cornu D, Miele P. Very Long SiC-based Coaxial Nanocables with Tunable Chemical Composition. Advanced Functional Materials 2007;17(16) 3251-3257.

[17] Huang ZM, Zhang TZ, Kotaki M, Ramakrishna S. A Review on Polymer Nanofibers by Electrospinning and Their applications in Nanocomposites. Composites Science and Technology 2003;63(15) 2223-2253.

[18] Chronakis IS. Novel Nanocomposites and Nanoceramics Based on Polymer Nanofibers Using Electrospinning Process-A Review. Journal of Materials Processing Technology 2005;167(2-3) 283-293.

[19] Shin DG, Riu DH, Kim HE. Web-type Silicon Carbide Fibers Prapared by the Electrospinning of Polycarbosilanes. Journal of Ceramic Processing Research 2008;9(2) 209-214.

[20] Eick BM, Youngblood JP. SiC Nanofibers by Pyrolysis of Electrospun Preceramic Polymers. Journal of Materials Science 2009;44(1) 160-165.

[21] Welna DT, Bender JD, Wei X, Sneddon LG, Allcock HR. Preparation of Boron-Carbide/Carbon Nanofibers from a Poly(norbornenyldecaborane) Single-source Precursor via Electrostatic Spinning. Advanced Materials 2005;17(7) 859-862.

[22] Guron MM, Wei XL, Welna D, Krogman N, Kim MJ, Allcock H, Sneddon LG. Preceramic Polymer Blends as Precursors for Boron-Carbide/Silicon-Carbide Composite Ceramics and Ceramic Fibers. Chemistry of Materials 2009;21(8) 1708-1715.

[23] Wu H, Sun Y, Lin D, Zhang R, Zhang C, Pan W. GaN Nanofibers based on Electrospinning: Facile Synthesis, Controlled Assembly, Precise Doping, and Application as High Performance UV Photodetector. Advanced Materials 2009;21(2) 227-231.

[24] Salles V, Bernard S, Brioude A, Cornu D, Miele P. A New Class of Boron Niride Fibers with Tunable Properties by Combining An Electrospinning Process and the Polymer-derived Ceramics Route. Nanoscale 2010;2 215-217.

[25] Eid C, Brioude A, Salles V, Plenet JC, Asmar R, Monteil Y, Khoury R, Khoury A, Miele P. Iron-based 1D Nanostructures by Electrospinning Process. Nanotechnology 2010;21(12) 125701.

[26] Wongtimnoi K. Polyurethanes électrostricitifs et nanocomposites : caractérisation et analyse des mécanismes de couplage électromécaniques. PhD thesis. Institut National des Sciences Appliquées de Lyon ; 2011.

[27] Martin DJ, Meijs GF, Gunatillake PA, McCarthy SJ, Renwick GM. The Effect of Average Soft Segment length on Morphology and Properties of a Serie of Polyurethane Elastomers. II. SAXS-DSC Annealing Study. Journal of Applied Polymer Science 1997;64(4) 803-817.

[28] Chen KS, Leon Yu T. Chen YS, Lin TL, Liu WJ. Soft and Hard-segment Phases Segregation of Polyester-based Polyurethane. Journal of Polymer Research 2001;8(2) 99-109.

[29] Koberstein JT, Russell TP. Simultaneous SAXS-DSC Study of Multiple Endothermic Behavior in Polyether-based Polyurethane Block Copolymers. Macromolecules 1986;19(3) 714-720.

[30] Dyre JC, Schroder TB. Universality of AC Conduction in Disordered Solids. Reviews of Modern Physics 2000;72(3) 873-892.

[31] Kremer F, Schönhals A. Broadband Dielectric Spectroscopy. Springer-Verlag; 2003.

[32] Su J, Zhang QM, Ting RY. Space-charge-enhanced Electromechanical Response in Thin-film Polyurethane Elastomers. Applied Physics Letters 1997;71(3) 386-388.

[33] Su, J, Zhang QM, Wang PC, MacDiarmid AG, Wynne KJ. Preparation and Characterization of Electrostrictive Films with Conductive Polymer Electrodes. Polymers for Advanced Technologies 1998;9(6) 317-321.

[34] Rybak A, Warde M, Beyou E, Chaumont P, Bechelany M, Brioude A, Toury B, Cornu D, Miele P, Guiffard B, Seveyrat L, Guyomar D. Synthesis of Polystyrene Coated SiC Nanowires as Fillers in a Polyurethane Matrix for Electromechanical Conversion. Nanotechnology 2010;21 145610.

[35] Galineau J, Guiffard B, Seveyrat L, Lallart M, Guyomar D. Study and Modeling of an Electrostrictive Polyurethane Diaphragm Loaded with Conductive Carbon Black. Accepted manuscript in Sensors and Actuators A: Physical http://dx.doi.org/10.1016/j.sna.2012.09.021.

[36] Fiorido T, Salles V, Seveyrat L, Hu L, Galineau J, Guiffard B, Brioude A, Guyomar D. Innovative Organic/Inorganic Nanocomposites for Actuators and Magnetic Sensors Applications. Submitted.

[37] Guyomar D, Yuse K, Cottinet PJ, Kanda M, Lebrun L. Focus on the Electrical Field-induced Strain of Electroactive Polymers and the Observed Saturation. Journal of Applied Physics 2010;108(11) 114910.